HDice Technical Note #24

Summary of the Feb'12 and Mar'12 eHD test runs

A.M. Sandorfi, A. Deur, M. Lowry, X. Wei, C.D. Bass
(last updated Mar 28, 2013)

Abstract

Two tests of the response of polarized HD to electron beams were conducted in 2012 during the course of the g14 run in Hall B. Polarizations were monitored with NMR. Measurements indicate several signal loss mechanisms at work. Calculations show that the beam raster system used in these tests was inadequate and resulted in significant heating of the target material, which could not be removed from the g14 target cells that had been optimized for photon running. The key features of these eHD tests are discussed here. A more comprehensive report is in preparation. A model that potentially accounts for most of the observations involves a combination of heat and ionization through Møller scattering, with effects compounded by ionization screening of the NMR RF response. These problems can be significantly mitigated with a high-speed raster and a different target cell design.

1.0 e+HD test runs in 2012

During opportunistic gaps in the g14 photon running, two tests were conducted with electron beams on polarized HD targets. Although conducted under less than ideal conditions, beams were rastered over the targets and studies were conducted with different raster areas, target temperatures and holding fields.

1.1 Feb'12 test run

This first eHD test was conducted between Feb 22 and Mar 2, 2012, using the g14 target #21a (*Silver*) and a 3 pass 3.3 GeV beam. Ten exposures to electron beams were carried out, interspersed with periods of NMR measurements. The rastered beam pattern was an ellipse during the first 3 doses (due to

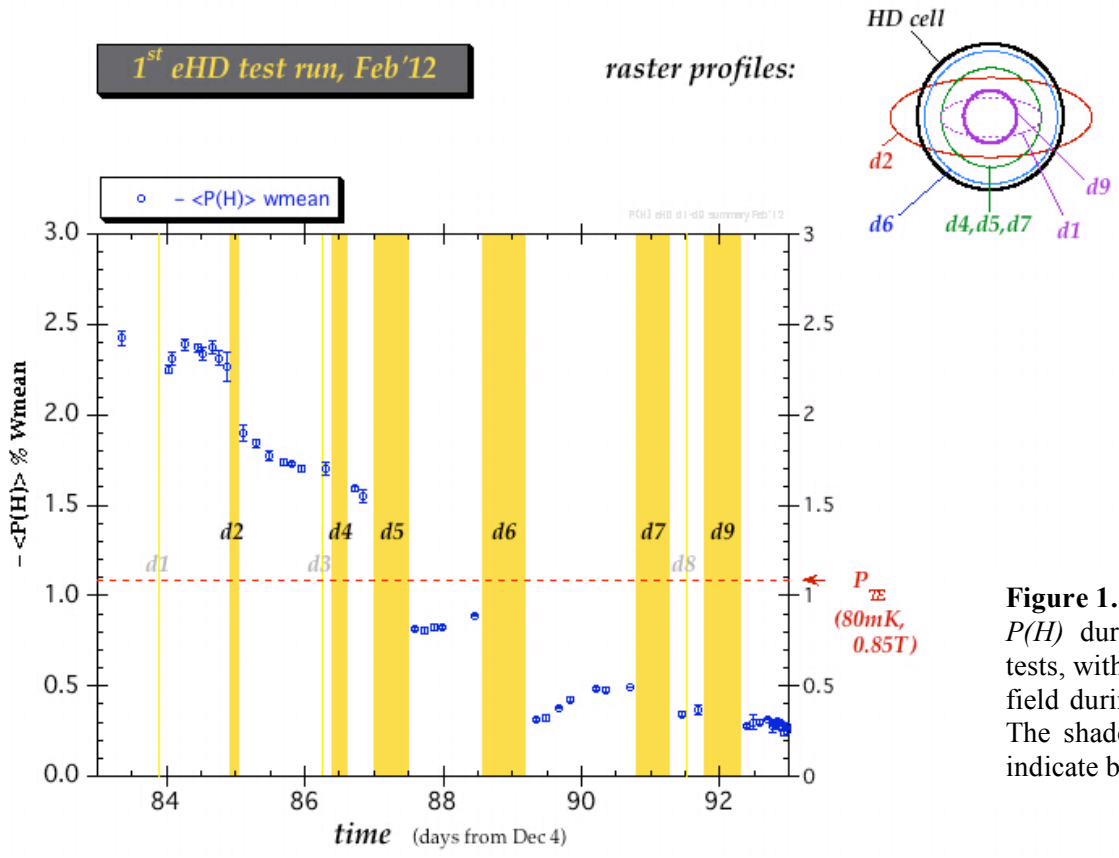

Figure 1. *P(H)* during Feb'12 eHD tests, with 0.9 tesla holding field during the exposures. The shaded vertical bands indicate beam-on periods.

incorrectly wired coils). This was fixed after the 3rd (very short) dose. The magnetic field was 0.85 tesla through the first nine doses. The characteristics of all doses are summarized in HDice-TN#23.
A graphical history of the H polarization is shown in figure 1 below together with a schematic representation of the raster size. The yellow bands in the graph indicate beam-on periods. The black circle in the upper right represents the cross section of the target cell; the different colored curves showthe size of the rastered beam on target to the same scale. Between dose exposures, many measurements were carried out at various magnetic fields and cryostat temperatures.

1.2 Mar'12 test run

This second eHD test was conducted between Mar 29 and Apr 1, 2012, using HD target 20b and a 5 pass 5.5 GeV beam. Two exposures to electron beams were carried out, interspersed with periods of NMR. The magnetic field was about 0.29 tesla throughout, which allowed field-sweep NMR data to be collected during the irradiation periods.

A graphical history of the H polarization is shown in figure 2 below. The black circle in the upper right represents the cross section of the target cell and the different colored curves show to the same scale the size of the rastered beam on target.

The first and second doses of this second period differed by a factor of 10 in current (100 pA vs 1 nA) and by about the same factor in polarization loss rate ($T_1(H)$ ~ 30 hr vs < 3hr).

This second eHD test period concluded with a search for radiation damage by turning off the holding field for an hour (day 18.2 in the plot above), with the intention of zeroing the polarization, restoring the field and then scanning NMR to see if any polarization grew back, which would indicate that the target was no longer in a frozen-spin state. On-line NMR analyses showed a growth of D polarization but no visible growth in H, suggesting that H was still in the frozen-spin mode, unaffected by electron

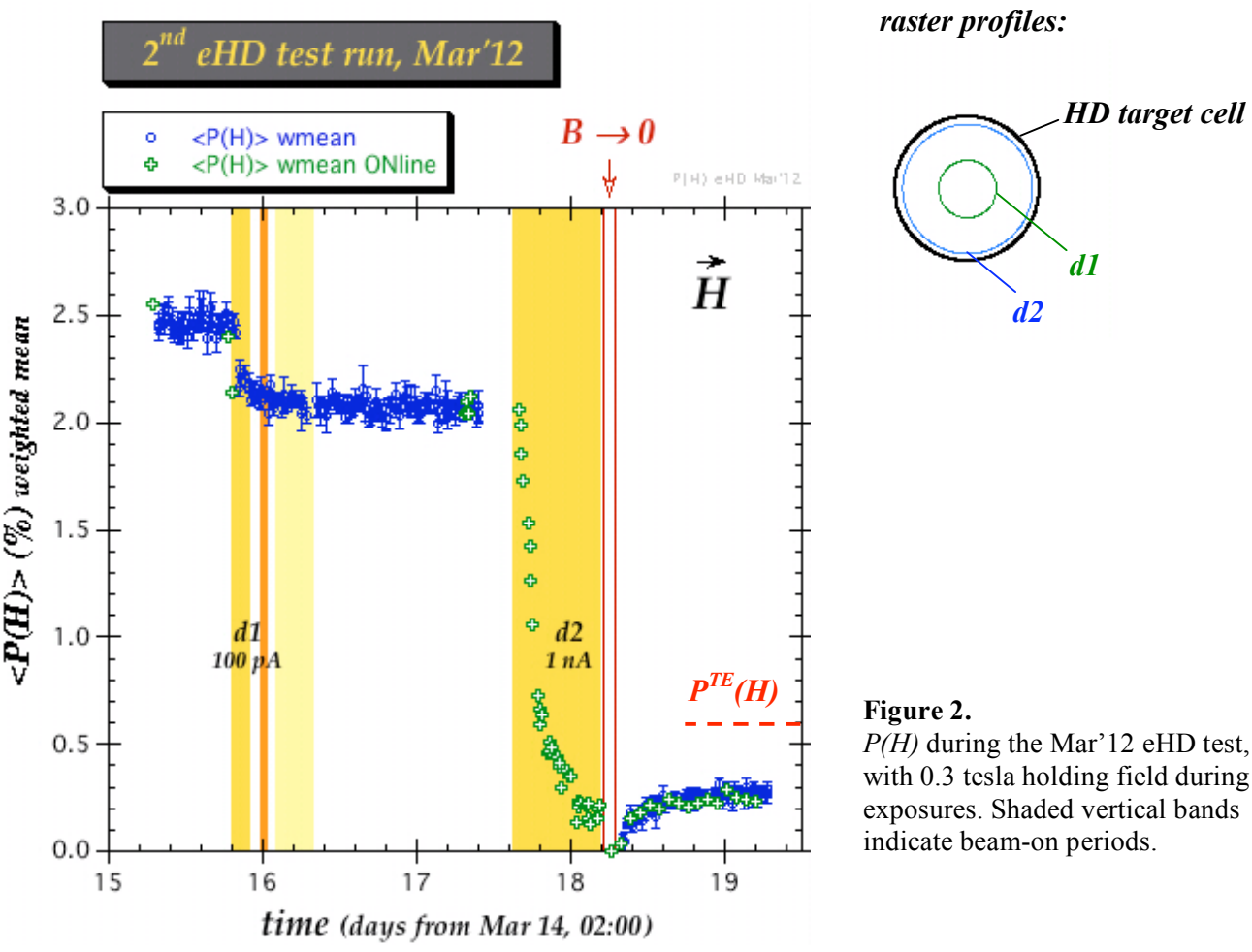

Figure 2.
P(H) during the Mar'12 eHD test, with 0.3 tesla holding field during exposures. Shaded vertical bands indicate beam-on periods.

bombardment. However, during subsequent off-line reanalyses of the NMR data last fall, a plotting error was discovered. The D and H NMR results after the field was zeroed had been interchanged. The corrected H polarization for the Mar'12 test is plotted in figure 2. After the field was zeroed at the end of the last dose, the H polarization did in fact start to grow back, but it stopped at about half of the expected Thermal Equilibrium (TE) value, suggesting that the frozen spin state had been recovered.

The D polarization showed a qualitatively similar behavior to H, although the signal loss rates with beam appeared higher. Here we concentrate on a detailed analysis of the H results.

2.0 Electron Beam interactions with the target

It is apparent in figures 1 and 2 that the polarization dropped when the beam was on target. Further changes in polarization followed with beam-off, although at a slower rate.

2.1 Electronic Effects of Beam Energy Deposition

Although the beam energy loss is dominated by Bremsstrahlung, the resulting photons primarily escape the target without interacting. Energy deposition within the target begins primarily with an elastic (Møller) scattering of a beam electron from a target electron. The energy sharing between the scattering electrons is generally highly asymmetric, the high energy one escapes the target while most of the low energy ones slow and stop, depositing their energy and falling into the HD conduction band. Alternatively, the scattered electron may be left in an anti-bonding orbital so that the HD molecule falls apart, the two atoms recoiling from each other to become interstitial impurities in the crystal lattice. In the first case we have electrons in the conduction band, which are free to respond to the RF field of the NMR measurement, and in either scenario we have unpaired electrons, which are magnetically active.

The cross sections for Møller scattering are shown below in figure 3. (Here we use the full relativistic calculation from [1].) The solid blue curve in the left panel indicates the part of the cross section having sufficient energy transfer to knock out a molecular electron. The integral of such curves are shown in the right panel for different beam energies. (Most of the integrated strength comes from the peak near 90 degrees; the spike at 0 degrees is in the beam but has little solid angle.)

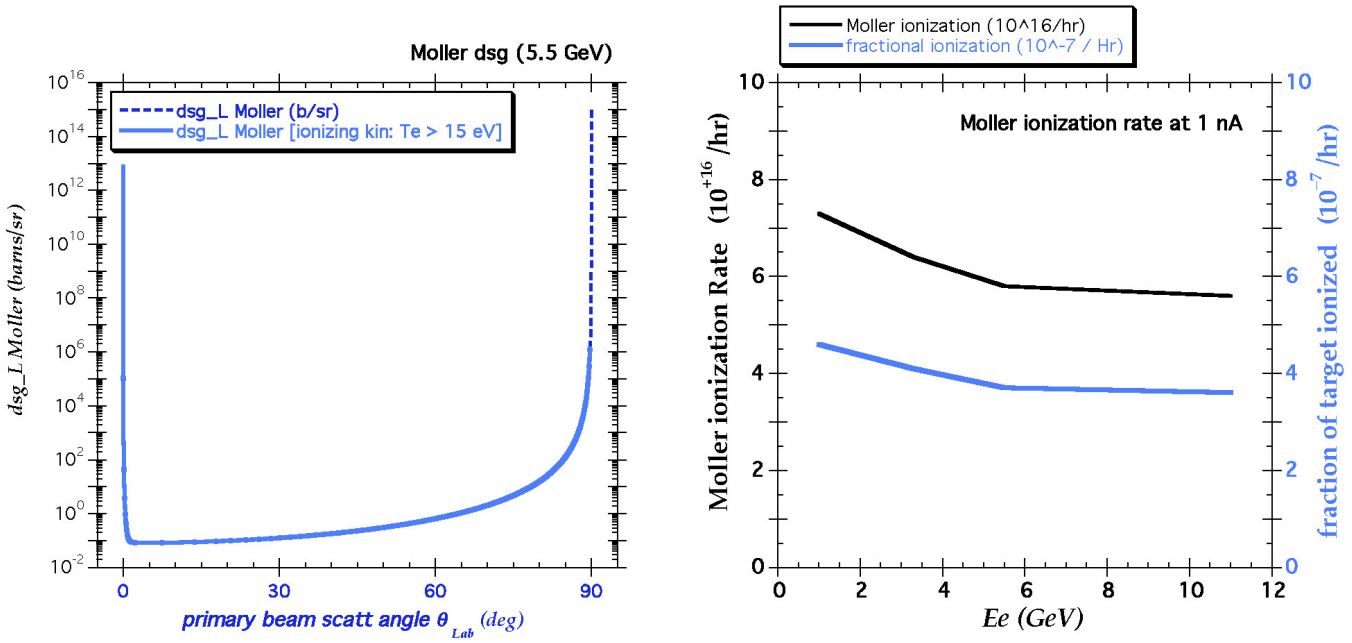

Figure 3. Cross sections for Møller scattering are shown in the left panel for a 5.5 GeV incident beam (dashed curve). That part of the cross section for which there is sufficient energy transfer to ionize HD (>15 eV) is shown as the solid blue curve in the left panel. The corresponding ionization rate for a 1 nA beam is plotted in black in the right panel. The associated fraction of the HD material a 15 mm ∅ × 50 mm g14 target cell that is ionized is plotted in blue (right panel).

2.2 Screening of the RF Field used for NMR

The HD minus ion is not stable, ejecting the electron to auto-neutralize. Thus, there is no intrinsic charge trap and a conduction band electron will roam the crystal until captured by an HD^+ ion. Electrons can enter the aluminum cooling wires but charge neutrality will demand their replacement. Similarly, electrons that were scattered out of the HD material will also be replaced by aluminum electrons entering the HD crystal conduction band. The net effect is a population of the conduction band which will reach an equilibrium, balancing the rate of population of the band through Møller scattering by the beam and the rate of capture on HD^+ ions, also created by the beam. This band population will respond to the RF field used to measure the NMR response of the target and partially screen it. This will result in a drop in the NMR signal, which occurs as the free charge builds up when the beam is put on target, and then a rise as the charge decays away after the beam is taken away.

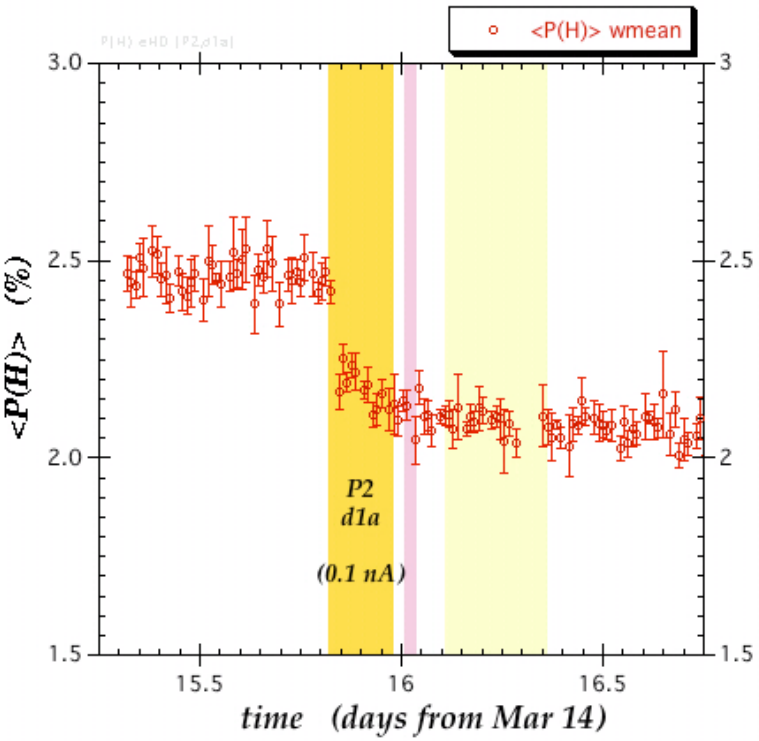

Figure 4. *P(H)* during test Period 2, the Mar'12 eHD run, with quasi-continuous NMR scanning. Shaded vertical bands indicate beam-on periods. Almost all of the 28 nA-min of this dose was accumulated in the first 3 hours, shaded deep-yellow and indicated as ***d1a*** (due to accelerator problems).

NMR scans were conducted every 15 minutes during the second test period, which provided a record of change during the doses. Both irradiations show a sudden drop in polarization in figure 2. The first dose is shown in an expanded scale in figure 4. Both here, as well as during dose ***d2*** visible in figure 2, the NMR signal shows an abrupt drop at the start of the exposure, followed by an apparent increase of T_1^H (a slowing down in the signal loss rate), which would be completely impossible for any real polarization loss mechanism. The initial drop in signal occurs as electrons enter the HD conduction band. Subsequent increases in T_1^H occurs as the molecular system approaches an equilibrium between the rate of band electrons falling back into bound HD orbits and the Møller repopulation of the band.

Once the beam-on period ended, the de-excitation of the conduction band and the associated removal of the NMR screening also explains the apparent increase in polarization after the end of the initial dose ***d1*** of Period 1 (figure 1). This first dose was very short (16 nA-min) and caused little real depolarization. From the regrowth data after ***d1***, the time constant for this *de-screening* is a few hours.

With such time constants of a few hours for depopulating an induced HD conduction band, signal loss from this screening process should dominate the short initial irradiations of each test period, ***P1,d1*** and ***P2,d1a***, where raster size and beam current were comparable. In fact, the signal loss from each of

these dose periods, **0.72 ±0.18** days and **0.98 ±0.20** days when expressed as a T_1, where $P_f = P_i \exp(\Delta t/T_1)$, are very similar despite the factor of 3 difference in magnetic field.

2.3 Signatures of Beam-Heating

We next search for evidence of depolarization effects due to the heat deposited in the target by the beam and examine their consequences.

Non-heat related polarization loss, due to changes in the local electronic structure of the HD lattice, should be proportional to the ratio of [incident charge] / [# exposed HD lattice sites] = {Q / raster volume}, or *Dose*. If this were the dominant process driving the polarization loss, then ***ΔP(H) / Dose*** should be a constant. This quantity is plotted for the various doses of the two test periods in the top panel of figure 5. The spread is evidently appreciable.

The other obvious factor that can potentially decrease polarization is heat due to energy deposited in the target by the beam. While the intrinsic beam spot is very small and capable of inducing significant

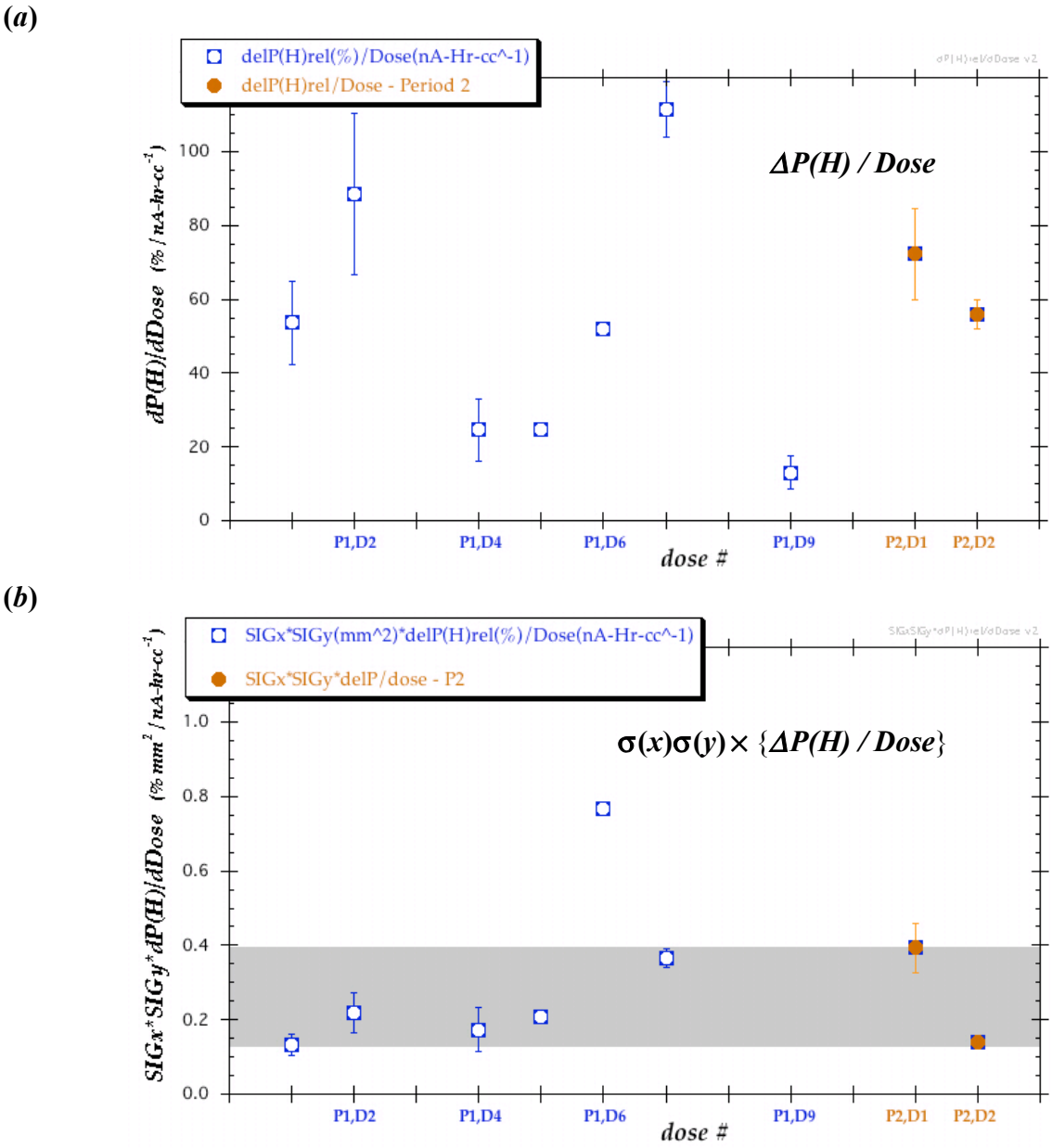

Figure 5. Change in H polarization per unit dose (charge/volume of the rastered beam envelope) is plotted in the top panel (*a*). Blue points are from the Feb'12 test period; gold are from the Mar'12 test run. Bottom panel (*b*) is the same quantity multiplied by the area of the intrinsic (unrastered) beam.

local heating, the Hall B spiral raster was used during the eHD test runs to spread the power over various fractions of the target, as indicated schematically in figures 1 and 2. (Details of this raster are given in [2]. Its calibration and settings for the Spring'12 tests are described in HDice Tech Note #23.) This was the only raster available at the time and, compared to the raster systems in Halls A and C, was relatively slow, requiring more than a second to complete a cycle. A slow raster cycle speed will result in a large amount of heat being dumped into a small cylinder of target material with cross sectional area determined by the beam spot. This can produce an additional component to polarization loss that is inversely proportional to the area of the intrinsic (unrastered) beam. In the bottom panel of figure 5 we plot $\boldsymbol{\sigma(x)\sigma(y)\times\{\Delta P(H)\,/\,Dose\}}$, using the one sigma values as measured in HARP scans for the beam dimensions. All but one point now lies in a relatively well defined band. (The outlier, **P**eriod 1 - **D**ose 6, is a particularly long exposure that had only one HARP scan a few hours before the start of the dose, none during and none until 2 days later. The beam was not very stable during these eHD test runs. Sudden polarization loss events had been observed correlated with beam motion. The *nanoAmp-BPM* that was usually positioned in front of targets in Hall B had been destroyed during the previous *2-photon* experiment, so the monitoring of beam motion and size was limited. Potential beam variations are more acute during long exposures. Since the beam size recorded prior to dose #6, and used for the evaluation in figure 5b, was uncharacteristically large, this could account for a higher value for the product $\sigma(x)\sigma(y)\times\Delta P(H)/Dose$ for *P1,d6* if the beam reverted to more typical dimensions later in the exposure.)

It is interesting that neither $\{\boldsymbol{\Delta P(H)\,/\,Dose}\}$ nor $\{\boldsymbol{\sigma(x)\sigma(y)\times\Delta P(H)}\}$ are constant. Only the quantity $\boldsymbol{\sigma(x)\sigma(y)\times\{\Delta P(H)\,/\,Dose\}}$ is an approximate constant, indicating that both the effects of heat and of radiation damage are present and are coupled. We will discuss several mechanisms for this below. But first we describe the results from a model for the heat deposition within the target to confirm the effect of the slow Hall B spiral raster.

2.4 Calculations of beam heating in the target

The structure of the g14 target cells used in the eHD test runs is shown schematically in the upper-left of figure 6. The HD consisted of a cylinder 15 mm diameter and 50 mm long, which was interlaced with approximately 900 aluminum wires (5N purity), each 38 μm diameter which reached 90 mm back to a copper cooling ring.

The Hall B Spiral raster used in the eHD test runs rotated the beam spot on target at a transverse speed of 3.1 m/s. Superimposed on this motion was a 1 Hz (max) amplitude oscillation which created a spiral pattern, shown schematically in the upper-right of figure 6. The modeled time evolution of HD temperature from a 1 nA beam is shown at the bottom of figure 6 for two radii, shown as blue and red circles in the upper-right schematic. The blue circle has half the radius of the raster area and is crossed twice in one cycle as the raster spirals the beam in and out, resulting in two temperature peaks. The red circles indicate regions near the limits of the spiral, at either the inner or outer edges. For these, the spiral motion crosses twice in rapid succession and the resulting temperature peaks are unresolved and appear as a single one.

These calculations assume the raster motion is limited to a 10 mm diameter circle, an average of the raster settings used in the two eHD test runs. The black dashed line in the plot below is the time average, the calculated temperature that would result from a 1 nA electron beam uniformly distributed across a 10 mm diameter cross section of the target. This 1 K temperature is determined by the limitations in the thermal conductance to the upstream copper heat sink. In principle, this has three components: the conductivity within the HD to the nearest Al wire, the Kapitza resistance at the HD-Al interface, and the thermal conductivity down the Al wire. The thermal functions used in these calculations of beam heating effects come from measured values reported in the literature. For aluminum, the thermal conductivity for normal state, five-nines aluminum from ref [3] is used. (Aluminum is super-conducting below 1.2K, but this is broken by the magnetic fields that surround the target.) For HD and for the Kapitza resistance, the results from ref [4] are used. (A correction has been applied to the Kapitza resistivity to account for

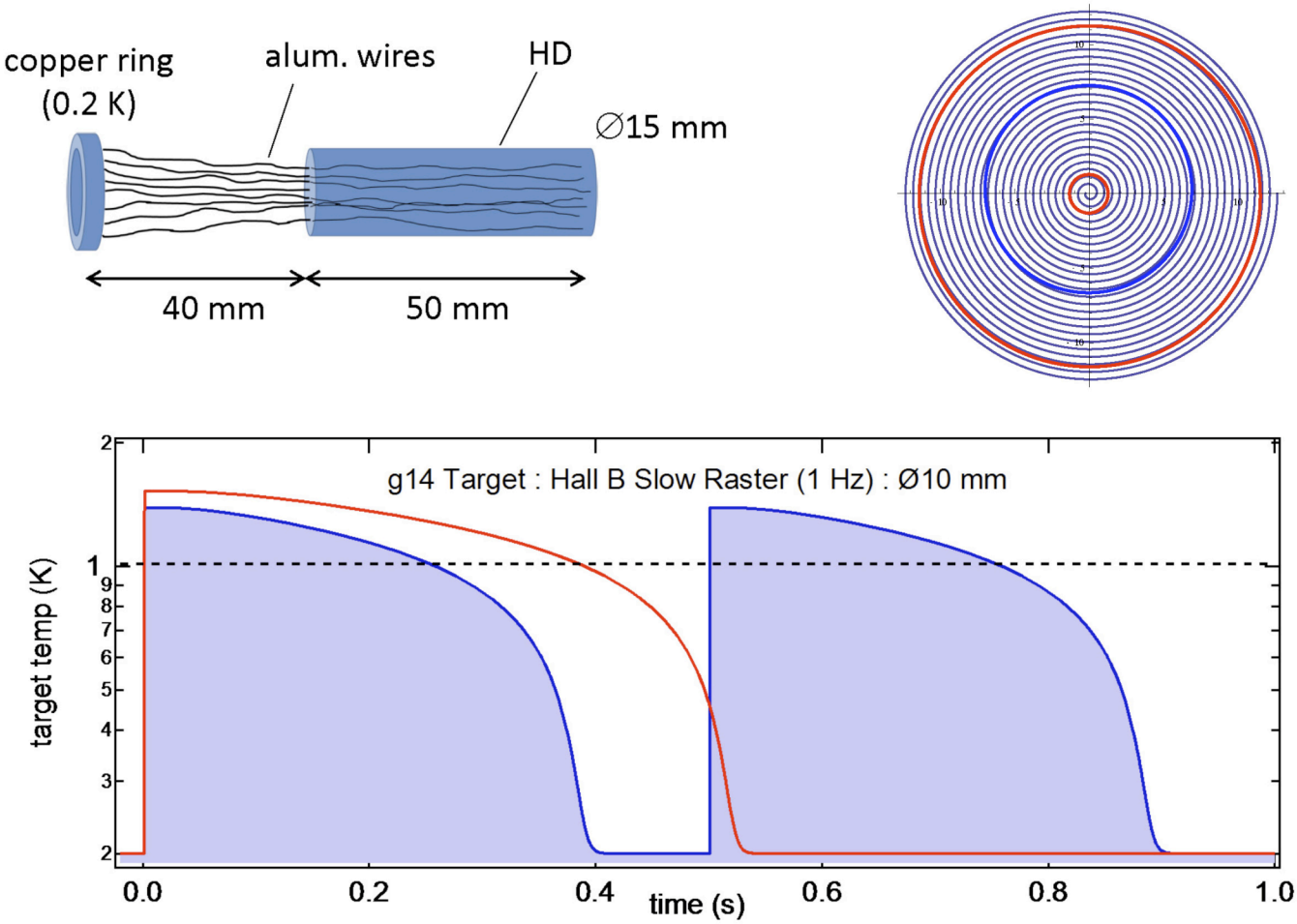

Figure 6. A schematic cross section of the target cells used in the 2012 eHD test runs is shown at the upper-left. The spiral pattern of the Hall B raster is shown schematically at the upper-right (not to scale). The calculated evolution of temperature in the HD from a 1 nA beam is plotted at the bottom for two radii, shown as blue and red circles in the upper-right schematic. The dashed line gives the expected temperature of a uniform electron distribution.

the density difference between the copper of the measurement and the aluminum in the target.) Table 1 shows the thermal resistivities at several temperatures. The much larger values of the HD thermal resistivity in Table 1 are potentially misleading because one must consider the geometry in determining the effective thermal resistance. If we use a simple planar geometry for comparison, the effect is to multiply by the distance along the heat flow and divide by the area transverse to it. For the aluminum, the relevant area is the cross-section of the wires and the characteristic distance is the target length. For the HD, the relevant area is the surface of the wires and the distance is that to the nearest wire. For the Kapitza resistance, it is the surface area of the wires that counts. The geometry is that of target #19b – 965 × 38-micron-diameter wires in a 15 mm diameter by 50 mm long target. This implies a wire cross-section of 1.1×10^{-6} m^2, a wire surface area of 5.7×10^{-3} m^2, and a maximum distance to a wire of 2.2×10^{-4} m. Table 2 shows the resulting thermal resistances.

Table 1: Thermal Resistivities at Several Relevant Temperatures

Temperature [K]	Al [m-K/W]	HD [m-K/W]	Kapitza [m^2-K/W]
0.800	0.00208	1.14	0.00095
0.200	0.00833	71.3	0.0608
0.020	0.0833	71250	60.8

Table 2: Effective Thermal Resistance at Several Relevant Temperatures

Temperature [K]	Al [K/W]	HD [K/W]	Kapitza [K/W]
0.800	95.2	0.044	0.165
0.200	381	2.77	10.57
0.020	3810	2770	10570

From Table 2, it should be clear that, in the temperature regime relevant for beam heating (0.2K and above), the aluminum is the dominant thermal resistance. Thus for calculations of beam heating effects, neglecting the HD and Kapitza resistances is a valid approximation that significantly simplifies the beam pulse calculations. For the target production temperatures around 0.020 K, no single component is dominate but only steady state calculations are necessary. Interestingly, the resistance of the HD itself has the smallest effect on its own temperature at all of the operating temperatures considered.
The other thermal property used in time dependent calculations is the heat capacity. For aluminum, we have used the measurements of ref [5]. In the case of HD, the results of ref [6] are used. For the same target parameters given above, Table 3 shows heat capacities at several temperatures and reveals that the HD is dominate around a Kelvin, while at the low polarizing temperatures the aluminum dominates.

Considering the above parameters, we obtain an understanding of the general behavior seen in figure 6 above. The peak of the heat pulse is dominated by the slow speed of the Hall B spiral raster. The long duration of the heat pulse(s), which keeps the average temperature high, is dominated by the resistance of the aluminum wires which, for the cell geometry used in the 2012 test runs, limited their ability to conduct away the beam heating. Because the HD heat capacity (in this case, its ability to give up its heat) drops with the cube of the temperature, as in Table 3, significant changes in power (electron current) are accompanied by relatively minor changes to the internal target temperature.

Table 3: Thermal Capacitance at Several Relevant Temperatures

Temperature [K]	Al [J/K]	HD [J/K]	Total [J/K]
0.800	$5.98\text{x}10^{-6}$	$9.32\text{x}10^{-4}$	$9.38\text{x}10^{-4}$
0.200	$1.48\text{x}10^{-6}$	$6.67\text{x}10^{-6}$	$8.15\text{x}10^{-6}$
0.020	$1.48\text{x}10^{-7}$	$6.15\text{x}10^{-9}$	$1.54\text{x}10^{-7}$

3.0 Polarization relaxation mechanisms

The HD material is among the simplest of molecules, having a structure similar to helium with two electrons paired in a *1s* orbital that generates no net spin or magnetic field. Møller scattering of beam electrons can transfer enough energy to break the *1s* pair, either creating an ionized HD^+ (15.4 eV) or dissociating the molecule into separate H and D atoms centered about the same lattice site (4.5 eV). The resulting electrons then become magnetically active.

3.1 Relaxation by Paramagnetic Impurities

The unpaired electron spin of the HD^+ ion, as well as the single electrons of dissociated atomic H and D, constitute isolated paramagnetic impurities, for which the theory of Rorschach should be applicable [7]. The basic mechanism assumes a constant rate of lattice-electron spin interactions, which can either flip or not flip the electron spin so as to bring the electron spin into thermal equilibrium at the current temperature and magnetic field. The dipole field of the electron flip, in turn, has a Fourier frequency component at the Larmor frequency of the surrounding nuclei. Thus the flip will occasionally relax a nuclear spin. This can lead to a spin relaxation of the target as a whole if the flip-affected nuclei can communicate with the rest of the target via spin-spin diffusion. But this diffusion is inhibited by the average magnetic field of the impurity electron, which can be sizeable at nearby lattice sites (more than

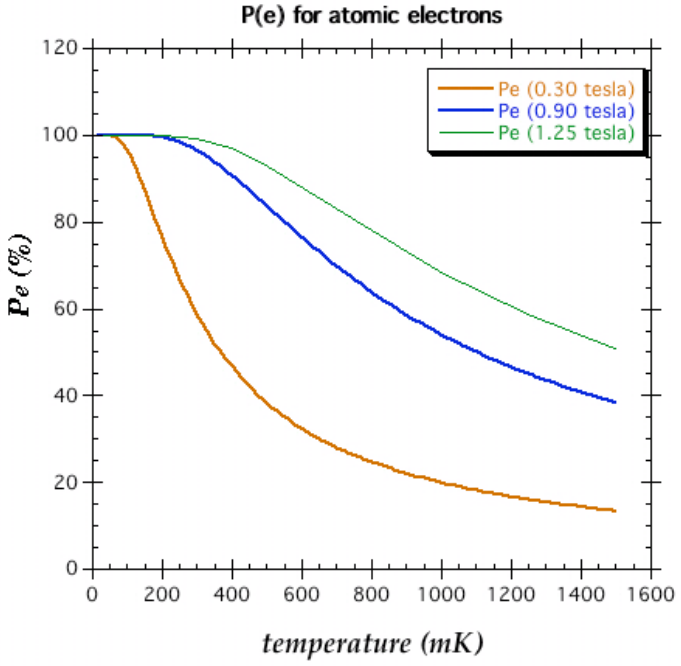

Figure 7. Electron polarization plotted against temperature for different external fields.

100 gauss at the position of its nearest neighbors) and so can result in shifts of the Larmor frequency of the nearby nuclei relative to the more distant ones. The average field is simply proportional to the impurity's electron polarization, which effectively quenches this nuclear depolarization mechanism. The calculated electron polarization is plotted in figure 7 against temperature for different external fields.

Rorschach puts all these effects together to predict, not T_1 itself, but how T_1 varies with temperature and field. This results in a nearly cubic field dependence to the polarization loss, as shown by the black dashed curve in figure 8. To comparison with data, we choose long exposures (9 hours) for which the NMR screening process (as well as charge-neutralization, which is discussed below) has come to an equilibrium, ***P1,d6*** and ***P2,d2***. These two doses were nearly identical, with a 1 nA beam rastered to the

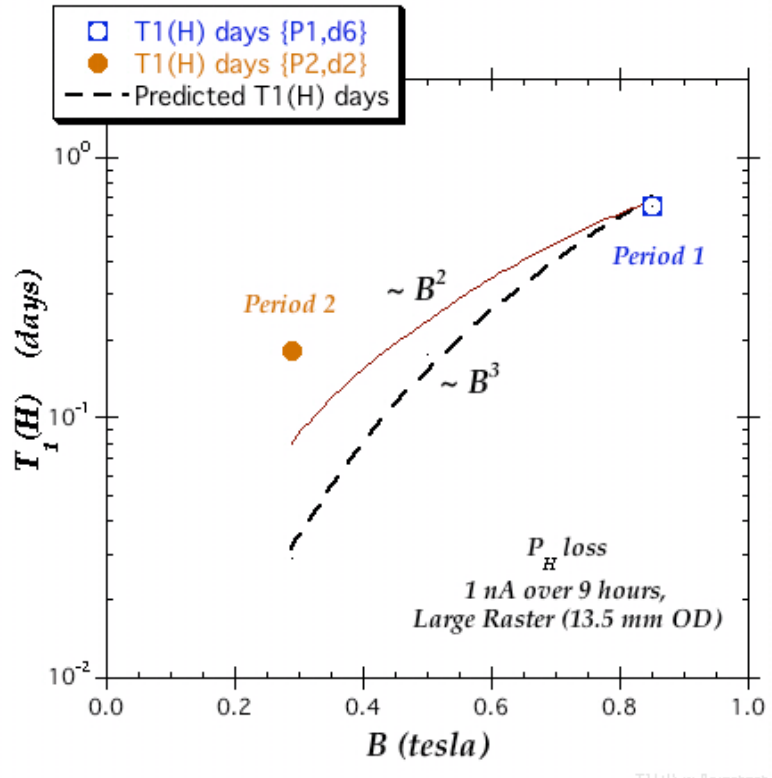

Figure 8. Polarization loss, characterized by the exponential time constant, T_1^H, where $P_f = P_i \exp(\Delta t/T_1^H)$. Results are shown from the period 1 (**P1**), at 0.85 tesla, and period 2 (**P2**), at 0.29 tesla, eHD runs in 2012. Other than magnetic field, the conditions in these dose measurements were nearly identical: 13.5 mm ∅ beam raster filling 81% of the target volume, 1 nA average current and 9 nA-hours of accumulated charge. (However, the size of the intrinsic unrastered beam spot was over 5 times larger for the period 1 datum.) The field dependence predicted by Rorschach [7] for depolarization by random flipping of electron spins, normalized to the high-field point, is shown as the black dashed line. The quadratic field dependence expected of hyperfine mixing is shown as the solid (red) line.

same size, filling 81% of the target volume. Essentially, the two irradiations differ only in their magnetic fields. The results are shown in figure 8, where the calculation has been normalized to the 0.9 tesla point. There is a significant drop in T_1 with magnetic field, although not as fast as predicted by the Roschach calculation.

3.2 Polarization Relaxation by Hyperfine Interactions

Another mechanism that can be at work in the presence of unpaired electrons is relaxation via the hyperfine interaction of a spin-½ electron with the spin-½ proton and the spin-1 deuteron. For the HD^+ ion, the electron-proton interaction energy is 0.93 GHz [8] and the electron-deuteron is 0.14 GHz. For atomic hydrogen, the hyperfine energy is 1.42 GHz and for atomic deuterium 0.33 GHz. These values can be compared to the electron spin splitting of 28 GHz /Tesla to see that we are in the high field (*Paschen–Back*) regime where the individual m-values are not "good" quantum numbers. The admixture of the opposite proton spin in the wave function of the HD^+ ion is 11% at the 0.29 Tesla field of Figure 2 and 4% at the 0.85 Tesla of Figure 1. This admixture varies inversely with the field and has no temperature dependence. From this, one expect T_1 to vary as B^2. However, in order to relax the target as a whole this wrong component must spin exchange with a nearby polarized nucleus to begin a spin-spin diffusion sequence, just as in the previous relaxation mechanism. Again, such diffusion will be inhibited by the average magnetic field of the electron, so that electron polarization, which depends on B/T, in fact comes into play. Thus for low temperatures, where the electron is fully polarized, we expect T_1 to vary as B squared and more strongly at higher temperatures where the electron is not fully polarized. A quadratic field dependence is shown as the solid red curve in figure 8.

4.0 Effects of the accumulation of static charge

The target cells can accumulate a net static charge as some of the Møller-scattered electrons leave the target. The net charge is neutralized over time by electrons from the aluminum wires. After an irradiation, once the HD is mostly neutralized, the crystal can regain its frozen spin state as the molecular *1s* electron orbitals become paired up. This is a possible explanation for the signal behavior at the end of the second dose period (figure 2). After the polarization was erased (by zeroing the holding field), the spin began growing back (via the relaxation mechanisms of section 3) but slowed dramatically when the material became essentially neutral again, with a net polarization that was about half of its TE value. The *1/e* time-constant of the rise in figure 2 is a few hours, comparable to the de-screening time, and large screening effects are evident during the second dose, making the final polarization value difficult to estimate.

We note that static charge in the form of HD^+ ions is not expected to contribute to NMR screening, since the charge is trapped in specific energy levels whose frequencies are very far from the Larmor frequencies of either H or D.

Charge neutralization can be fairly rapid for ionized sites that are near aluminum wires. But as the distance to a wire increases, the time constant for neutralization could increase markedly. The number of such *remote* sites capable of retaining a charge for long periods (longer than the few hours of the rise evident in figure 2) will increase with total accumulated dose. Polarization decay constants (T_1) were measured in between the irradiations of the first test period (figure 1) under various conditions of holding field and cryostat temperature. The results are plotted in figure 9. Since the effects of signal screening and static charge buildup had not been anticipated, these data were measured at different intervals of time after the end of each irradiation. As a result, their values are a mixture of the different signal loss mechanisms discussed above. Nonetheless, there is a consistent drop (shortening of the apparent spin relaxation time) with accumulated beam-off dose.

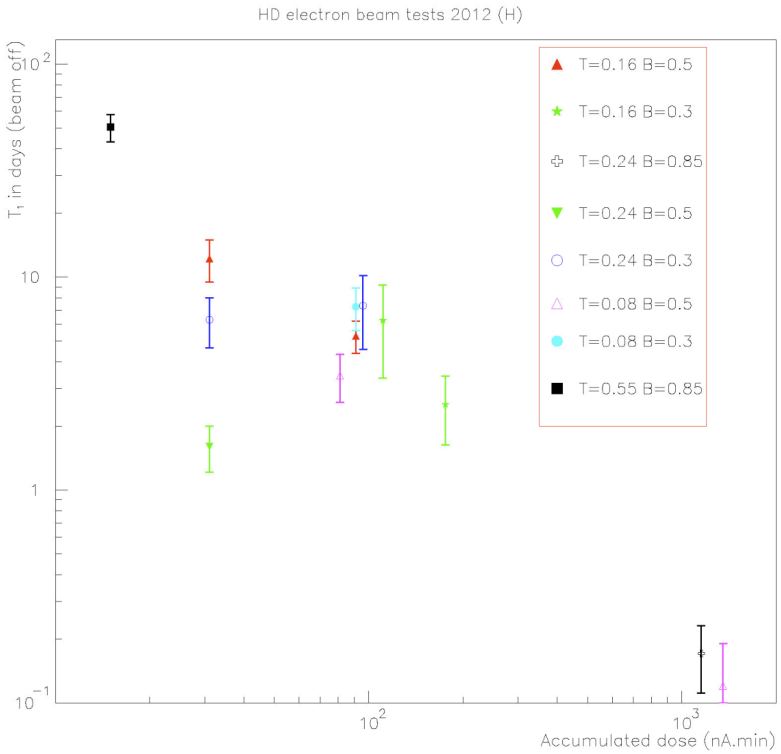

Figure 9. Polarization decay constants for hydrogen, T_1 where $P_f = P_i \, exp(\Delta t/T_1)$, as a function of accumulated dose, as measured in between doses under various conditions of holding field and temperature. (See text.)

5.0 Comparisons with eHD Test Data and Outstanding Questions

For the doses of the first test period plotted in figure 1, the magnetic field was held at 0.85 tesla during the dose irradiations and NMR measurements (at 0.29 tesla) were taken before and after each dose. During the two doses of the second test period of figure 2, the field was kept at about 0.29 tesla as NMR sweeps were made in 15 minute intervals throughout the beam-on dose periods. These two conditions correspond to the blue and gold curves in figure 7, respectively. In both cases, for target temperatures in the expected 1 Kelvin region (figure 6), Møller-unpaired electrons are far from fully polarized (52% and 19%, respectively). As a result, the HD polarization loss could not be quenched as discussed in the previous section. While this put the polarization loss in a complex regime with several competing processes, at least qualitative comparisons with the data are on the whole quite successful.

For example, the current during the first dose of the second test period (figure 2) was 0.1 nA, a factor of 10 lower than the 1 nA of the second dose. Nonetheless, because of the known cubic temperature dependence of the heat capacity (Table 3) the resulting target temperature (~ 0.58 K) was less than a factor of 2 lower than the ~1 K of the higher current run. At 0.58 K and 0.3 tesla, the electron polarization was still quite low during the first dose (figure 7), which resulted in significant polarization loss despite the apparent large reduction in current. The rate of loss should be proportional to the number of unpaired electron sites available to relax an H and that should be proportional to current. Indeed, the T_1^H loss rates for these two doses differ by about 10.

Despite a large measure of understanding in the main results of the eHD test runs, the last test of figure 2, the regrowth after zeroing of the external field, continues to have puzzling features.

- With beam-off, the temperature and field conditions of 55 mK and 0.29 tesla would have produced an electron polarization of 99.84%. At this level, the expectation from the Rorschach calculation (section 3) would be a decoupling of the electron spin from the *p* and *D* spins, in which case the HD should have remained in a frozen spin state with zero polarization and P(H) should not have grown back.

- If the polarization regrowth mechanism involved dissociated (but neutral) H and D atoms at a common lattice site, their recombination rate would have to be rather specifically tuned to stop the growth at ½ of the TE value. (Of course, the same can be said of charge neutralization.)
- There is another aspect of the NMR response that is puzzling and still under investigation. When the holding fields are adiabatically rotated from $+z$ (along the beam axis) to $-z$, the NMR signal appears to drop to about 60% of its $+z$ value, suggesting a loss of polarization. However, when the procedure is repeated and the spins are rotated back along $+z$, the original NMR signal is mostly restored. One possible explanation is the presence of some as yet unidentified source of magnetic field in the vicinity of the target. If such an additional field source were present, it could have preserved the target spin, or at least limited its loss during the short period after ***P2,d2*** (figure 2) when the main solenoid was turned off for an hour. The presence of significant screening during ***P2,d2*** makes it difficult to know the real polarization at the start of the hour with zero solenoid current. In this case, the apparent rise in signal could reflect the decay of screening as electrons leave the HD conduction band. The difficulties in interpreting this result are compounded by charge neutralization, which surely is also taking place.

6.0 The next generation electron target

In all scenarios, heat plays a significant roll in the results of the 2012 eHD test runs. The high temperatures in the test conditions (figure 5) arose from the geometry of the g14 target cells in which the conduction down the aluminum wires and the slow speed of the Spiral Raster limited heat removal. It is also clear from the measurements that the polarization loss rate is coupled to the number of Møller scattering sites. Both of these issues are very significantly mitigated in the new design shown schematically in figure 10. The target cell has been shortened, minimizing the lengths of the aluminum

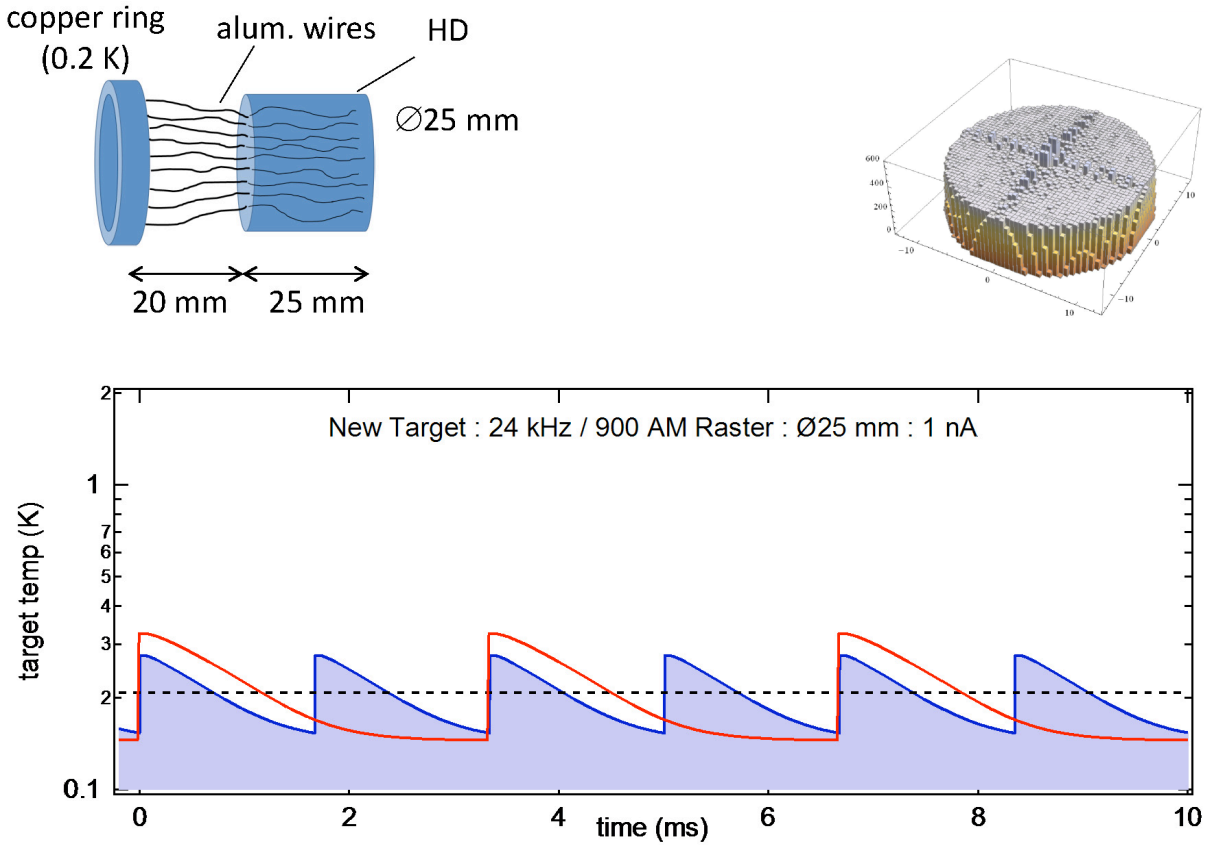

Figure 10. A schematic cross section of the next generation target cell planned for a future eHD test run is shown at the upper-left. The raster system assumed here is the Hall A (or C) *Fast Raster*, operating at 24 KHz with a 900 Hz amplitude modulation. The calculated evolution of temperature in the HD from a 1 nA beam is plotted at the bottom for two radii, one at mid-radius (blue) and the other near the inner or outer limits of the pattern (red). The dashed line gives the expected temperature of a uniform electron distribution. (Note the difference in the time scale when comparing to figure 5.) The raster uniformly fills the target, as in the simulation in the upper right.

cooling wires. At the same time, the diameter of the HD has been increased from 15 mm to 25 mm. The dimensions are shown in the upper-left of figure 10. The simulated internal heat is based on one nA of current, spread over the target using the existing 6 GeV raster systems that have been used in Halls A and C. Operating at 24 KHz with 900 KHz amplitude modulation, this would produce a transverse speed of 1885 m/s and result in a pattern refresh rate that is a thousand times more rapid than the Slow Spiral raster of figure 5. (Note the different time scales in the two figures.) With this configuration, the average temperature of the HD can be reduced to 208 mK.

6.1 Next generation performance estimates from scaled behavior

While open questions remain, we can make an estimate of the polarization lifetime for the new target raster combination of figure 10 with the following observations:

- The diameter of the new cell is 25 mm, compared with the 15 mm ∅ of the g14 cells. The number of HD sites increases with the square of this dimension so that, for the same current, the density of affected HD sites drops by a factor of $(25/15)^2 = 2.8$.
- With the fast raster and the cell geometry in figure 10, the calculated average temperature of the HD is expected to be 208 mK. This should be compared to 735 mK for the slow raster filling the g14 target. (This is lower than the 1 K of figure 5, where a mean raster cross section of 10 mm ∅ was assumed.) There are various interconnected effects that are influenced by temperature, with dependences that can be dramatic. A simple linear dependence would suggest an improvement of $(735/208) = 3.5$.

⇒ Applying these enhancements to the 0.9 tesla datum of figure 9 would suggest a T^1_H of 6.4 days at 1 nA.

⇒ A modest increase in holding field to 1.2 tesla would suggest a T^1_H of 9 days at 1 nA.

Either of these conditions would imply a viable target for electron experiments.

7.0 Summary and Conclusions

The two 2012 eHD tests conducted during opportunistic gaps in the g14 photon running were carried out in far less than optimal conditions.

- the Hall B *Spiral Raster*, the only raster available at the time, proved to be far too slow and allowed the beam to increase the target temperature excessively;
- the g14 target cells were optimized for the photon experiment and could not efficiently conduct away electron beam-heating, with the result that the higher temperatures lingered within the target for most of the raster cycle;
- the beam diagnostics were poor, since the electronic readout of the beam position monitor before the target had been destroyed during the previous *2-photon* experiment.

While the space of the parameters affecting HD polarization when exposed to electron beams has proved to be quite complicated, the creation of HD^+ ions by the beam and the interactions with the spin of the ions' unpaired electron is capable of accounting for most of the observed polarization losses. These losses are expected to be greatly reduced when the unpaired electrons are highly polarized, a condition that could not be achieved in the 2012 eHD test runs due to the high target temperatures.

Straight-forward improvements in the target cell and the raster are expected to drop the internal HD temperature significantly. Scaling from test results, these improved conditions should result in polarization lifetimes of about a week at 1 nA. This would provide a viable target for the approved transverse polarization experiments. Nonetheless, given the many competing processes in play, further testing is essential.

[1] J.M. Jauch and F. Rohrlich, *The Theory of Photons and Electrons*, Springer-Verlag, New York (1976)

[2] F.J. Barbosa, *Raster Hall B – Spiral User's Manual*, v 1.0, September 2000.

[3] O.V. Lounasmaa, *Experimental Principles and Methods Below 1K*, Academic Press (1974) p246

[4] J.H. Constable and J.R. Gaines, Phys. Rev **B8** (1973) p3966

[5] N. Phillips, Phys Rev **114** (1959) p676

[6] J.H. Constable, A.Q. McGee and J.R. Gaines, Phys. Rev. **B11** (1975) p3045

[7] H.E. Rorschach, Physica **30** (1964) 38

[8] D. Bakalov, V.I. Korobov and S. Schiller, Phys. Rev. Lett. **97** (2006) 243001